Article

Optical Signal Attenuation through Smog in Controlled Laboratory Conditions

Hira Khalid [1,*], Sheikh Muhammad Sajid [1], Muhammad Imran Cheema [2], Erich Leitgeb [3,*]

1 Department of Electrical Engineering, National University of Computer and Emerging Sciences, Lahore 54000, Pakistan; sm.sajid@nu.edu.pk
2 Department of Electrical Engineering, Syed Babar Ali School of Science, Lahore University of Management Sciences, Lahore 54792, Pakistan; imran.cheema@lums.edu.pk
3 Institute of Microwave and Photonic Engineering, Graz University of Technology, 8010 Graz, Austria
* Correspondence: khalid.hira28@gmail.com (H.K.); erich.leitgeb@tugraz.at (E.M.)

Abstract: Free-space optical (FSO) communication is a line-of-sight (LOS) communication technology that uses light, typically lasers, to transmit data through the atmosphere. FSO can provide high data transfer rates, but factors like weather conditions can affect its performance. Like fog, smog also degrades the availability and reliability of FSO links, as the particulate matter (PM) present in smog scatters the light beam, causing perceptible attenuation. In this paper, we have investigated the attenuation of an optical signal under laboratory-controlled smog conditions, using both theoretical and experimental approaches. A 6 m long acrylic chamber is used to contain artificial smog and measure the optical attenuation through it. The experimental result shows that smog attenuation is approximately 1.705 times more than fog attenuation. The findings of this study offer valuable insights into the effects of smog on optical links and can contribute to the development and optimization of these systems in regions with high levels of smog.

Keywords: smog attenuation; visibility; free-space optics

1. Introduction

Free-space optics (FSO) is a communication technology that utilizes optical signals to transmit data wirelessly through the atmosphere, without the need for physical cables or wires. It is also known as optical wireless communication (OWC), and it employs infrared and visible light for transmission. FSO has several advantages over traditional communication methods, including high data transmission rates, low latency, and immunity to electromagnetic interference (EMI) [1–3]. It is also a cost-effective solution for transmitting data over short distances, and it can be used in various applications, such as last-mile connectivity, building-to-building communication, and disaster recovery. FSO systems consist of a transmitter and a receiver that use optical lenses to focus the light beam on the receiver. The signal is modulated onto the beam of light, and the receiver detects the modulated signal and demodulates it to retrieve the original signal. The beam of light can travel through the atmosphere, but it is subject to atmospheric attenuation, which can cause signal loss.

In recent years, FSO has gained popularity in the telecommunications industry, and it is being considered as a complementary technology to traditional wired and wireless communication methods. With the increasing demand for high-speed, reliable, and cost-effective communication solutions, FSO is expected to play a substantial role in the future of wireless communication in 5G systems. FSO has a few disadvantages, like it requires precise alignment between the transmitter and the receiver. Small movements or vibrations can disrupt the alignment and cause signal loss. Atmospheric conditions such as fog, rain, and snow can affect the performance of FSO systems by causing signal attenuation [4,5]. However, using adaptive optics, tracking systems, and encryption techniques can help

mitigate the effects of atmospheric attenuation [6,7]. FSO is a rapidly developing technology with the potential to revolutionize the way we communicate. Several organizations, such as the International Telecommunication Union (ITU), have developed standards and guidelines for FSO technology. As the technology continues to mature, we can expect to see FSO systems used in even more applications.

Researchers in 2009 achieved a data rate of 1.28 Terabits/sec with six hours of stability and no burst errors. The system utilizes saturated EDFAs to improve signal power stabilization [8]. A team of researchers conducted experiments to evaluate the performance of FSO links under adverse weather conditions, such as fog, rain, and snow. They found that the availability of FSO links is significantly affected by atmospheric attenuation and is wavelength-dependent [9]. In [10], the authors proposed a new model based on the Monte-Carlo simulation and Kim formula to enhance the link budget analysis and guide the parameter design in foggy conditions. Researchers, in [11], proposed that FSO communication can be optimized by using variable transmitted power controlled by a visibility detector to overcome the impact of different weather conditions, ultimately enhancing system performance. Attenuation of terrestrial and satellite signals over George, Western Cape in South Africa was studied in [12]. The researchers collected meteorological data for visibility over a ten-year period and calculated the total optical attenuation. A new wavelength-independent method for estimating attenuation in FSO links based on visibility measurements was proposed in [13]. The study considers four locations with different climate conditions and shows that the results obtained align with micro-physical models. In another study [14], adaptive modulation and coding schemes for FSO links were proposed to improve the performance of the links in variable atmospheric conditions. The proposed schemes adjust the modulation and coding parameters based on the signal-to-noise ratio (SNR) of the link and also improve the bit error rate (BER) performance of FSO links. Many scholars proposed hybrid FSO-RF systems, which combine the advantages of radio frequency (RF) communication and FSO to provide reliable and high-speed communication links. The proposed system uses FSO links as the primary communication link and RF links as the backup link, to provide a seamless communication channel [15].

The rapid expansion of urban areas and industrialization has led to an alarming increase in air pollution levels worldwide. One of the critical components of air pollution is smog, a complex mixture of particulate matter (PM), gases, and aerosols, often exacerbated by factors, such as vehicle emissions and industrial activities. Smog not only poses significant health risks to humans but also exerts adverse effects on various technological systems, including communication networks. There are different research works conducted for measuring fog and smoke attenuation, but to the best of our knowledge, smog attenuation is not exclusively studied for the optical signal. In this research paper, we delve into the distinctions between fog and smog, exploring their unique characteristics, causes, and consequences. We aim to comprehensively investigate the impact of smog on FSO communication in controlled laboratory conditions using artificial smog. The primary objective of this experiment is to quantify the extent of optical signal attenuation induced by varying densities of smog. The results endeavor to provide valuable insights for the development of robust FSO systems, capable of withstanding smog-induced challenges in real-world applications. Taking outdoor measurements for smog attenuation proved challenging due to the potential harm posed by lasers to human eyes. The task encompassed navigating the selection of the deployment site and addressing the limited availability of long-distance lasers suitable for the purpose. Therefore, we considered an indoor transparent acrylic chamber of a length of 6 m to take real-time measurements. We investigated smog attenuation for FSO links operating at wavelengths of 780 nm and 1550 nm and its dependency on meteorological visibility. The results for smog attenuation are compared with smoke and fog attenuation to develop a better understanding of the scattering of light beams through different mediums. The values for optical attenuation can be obtained by exploring the impact of different weather conditions on FSO systems, drawing insights from the existing studies present in the literature [16–18]. The rest of this paper is divided as follows: the

FSO analysis of the smog channel is in Section 2, the experimental setup is outlined in Section 3, and the results are discussed in Section 4.

2. FSO Analysis in Smog Channel

2.1. Smog

Understanding the difference between fog and smog is essential for several reasons. Firstly, it allows for the accurate identification and classification of atmospheric conditions, aiding in meteorological forecasting and public safety measures. Secondly, recognizing the variation in composition, formation mechanisms, and geographical distribution enables the development of targeted strategies to mitigate the specific impacts of fog and smog.

Smog formation is primarily attributed to the interaction of pollutants with sunlight and atmospheric conditions. It involves complex photochemical reactions that result in the creation of secondary pollutants and the formation of haze-like air pollution. Photochemical smog, the most common form of smog in urban areas, is formed through a series of chemical reactions [19]. It starts with the emission of nitrogen oxides (NO_x) and volatile organic compounds (VOCs) from vehicle exhaust, industrial processes, and other human activities. These pollutants react with sunlight, leading to the production of ground-level ozone (O_3) and other secondary pollutants, such as formaldehyde, acrolein, and peroxyacyl nitrates (PANs). The presence of temperature inversions, where a layer of warm air traps pollutants near the surface, exacerbates the formation and accumulation of smog. Classic smog, prevalent in industrial areas, is primarily a result of coal combustion and industrial emissions. It involves the release of sulfur dioxide (SO_2), particulate matter (PM), and other pollutants that combine with moisture to form smog. The combustion of fossil fuels like coal releases sulfur dioxide, which reacts with atmospheric moisture to form sulfuric acid aerosols, contributing to the characteristic hazy appearance of classic smog. The formation of smog is influenced by many factors, such as the source of pollutant emissions, sunlight intensity, temperature inversions, and atmospheric stability. Smog tends to be more prevalent in densely populated urban areas with high levels of industrial activities and vehicular emissions [20].

Smog is known to have a detrimental effect on visibility, making it difficult to see over long distances. The pollutants in smog, such as particulate matter, can scatter and absorb sunlight, causing a reduction in visibility. The meteorological definition of visibility is "the distance that a beam of light travels until its luminous flux decreases to 5% of its initial value" [21].

2.2. Characterization of Smog Attenuation

Smog typically contains ($PM_{2.5}$) particles depending upon the source of pollution. For such a particle size, Mie scattering is considered with the aerosol refractive index given as $\epsilon = \epsilon - j\epsilon_i$, where the real part shows scattering and the imaginary part shows absorption. Moreover, the absorption coefficient is given by $x = 2\pi a/\lambda$, i.e., the ratio of the circumference of the particle to the operating wavelength λ. Assuming that the smog particles are symmetrical and spherical in shape, we can apply the exact Mie theory to calculate the normalized scattering and absorption efficiencies. But for FSO, we normally use typical wavelengths like 780 nm, 950 nm, and 1550 nm for which molecular absorption is minimal. So, we will only consider normalized scattering efficiency, which is given by [22]:

$$Q_s = \frac{C_s}{\pi a^2} \tag{1}$$

where Q_s is a unit less quantity with a maximum value reaching 3.8 for the maximum scattering of the optical beam. C_s is the scattering cross section of particles of radius r. The optical signal strength deteriorates as it travels through a distance l by $e^{-\gamma_s l}$, where γ_s is given by $\gamma_s = N\pi a^2 Q_s$. If $N(a)da$ particles have radii between a to $a + d(a)$ per unit volume, then

$$\gamma_s = \int_0^\infty Q_s N(a)\pi a^2 da \tag{2}$$

The particle distribution is generally represented by some analytical model, such as gamma–gamma distribution. Empirical models are used to predict the attenuation of the optical signal, which utilizes visibility data for its estimation. The modified Koschmieder relation is used to calculate the extinction coefficient using visibility data, which is given by $\beta_{ext-vis} = 1.9/Visibility$. Moreover, to study the effect of $PM_{2.5}$ on aerosol extinction, a modified IMPROVE model can be used to calculate the atmospheric extinction coefficient as [23]:

$$\beta_{\text{ext}} = 3f(\text{RH})[\text{SULPHATE}] + 3f(\text{RH})[\text{NITRATE}]$$
$$+ 4[\text{ORGANIC CARBON}] + [\text{SOIL}] + 0.6[\text{COARSE MASS}] \tag{3}$$

where $f(RH)$ are the growth factors of relative humidity and the brackets show the mass concentration of each component in μgm^{-3}. The visibility (V) in km can be expressed as $V = -10\log_{10}(T_{th})/\gamma_\lambda$, where T_{th} is supposed to be 5% and γ_λ is given by the Beer–Lambert Law as [22]:

$$\gamma_\lambda = -\frac{10\log_{10}(T)}{4.343L} \tag{4}$$

where T is the transmittance of the optical signal. Researchers, in [22], claim that the Kim model does not account for the wavelength to calculate the attenuation for $V < 0.5$ km. So, using the empirical curve-fitting method, they have calculated the value of q as:

$$q(\lambda) = \begin{cases} 0.1428\lambda - 0.0947 & \text{Fog} \\ 0.8467\lambda - 0.5212 & \text{Smoke/Smog} \end{cases} \tag{5}$$

and suggested a modified version of the Kim model as:

$$\beta_\lambda(dB/km) = \frac{17}{V(km)}\left(\frac{\lambda}{\lambda_o}\right)^{-q(\lambda)} \tag{6}$$

where λ_o = 550 nm is the maximum sensitive wavelength for the human eye. This model is valid for 0.015 km$< V < 1$ km and 500 nm$< \lambda <$1600 nm. For the scope of our research, smog can be considered the closest match to the smoke in terms of its composition. So, the modified Kim model and its value of q can be used for modeling the smog optical channel.

3. Experimental Setup

A block diagram of the experimental setup for the FSO link through artificially generated smog is shown in Figure 1. The laboratory setup consists of a laser, photo-diode, smog machine, and custom-designed 6 m sealed acrylic chamber with precise control mechanisms for introducing smog constituents. Fans are used to achieve homogeneity of the artificially generated smog throughout the chamber. A mixture of nitrogen oxides and volatile organic compounds is injected into the chamber using a smog machine to emulate smog conditions. UV lights are used for a limited time to produce small amounts of secondary pollutants, like formaldehyde. All precautionary measurements are considered while conducting the experiments. The aerosols are slowly moving fine particles suspended inside the chamber. It is observed that increasing the observation length can reduce the effect of any non-homogeneous smog patches inside the chamber. A small change in the density of aerosols can cause a significant change in the value of β_γ as given by Equation (6). Two different approaches are used to characterize the smog attenuation, (i) based on different levels of visibility and (ii) different values of operating wavelengths, i.e., 780 nm and 1550 nm. At T = 0, we measure the link attenuation before the smog injection and mark its value as a reference for further reading. Artificial smog is then injected inside the chamber through a vent hole and allowed a time of 5 minutes to spread homogeneously before acquiring data points again. The smog density is controlled using air outlets to create dense to very light smog inside the chamber. The received optical power is measured

using THORLABS PM320E constantly until the chamber is free from smog. The geometric and reflection losses from the walls of the chamber are not considered as the received power is measured for both with and without smog. The normalized transmittance T is determined by the ratio of the received power without smog to the received power with smog. This experimental procedure is followed to acquire datasets for both 780 nm and 1550 nm using THORLABS CLD-1015 and Santec WSL-100 lasers, respectively. Figure 2 shows the experimental setup to measure the smog attenuation.
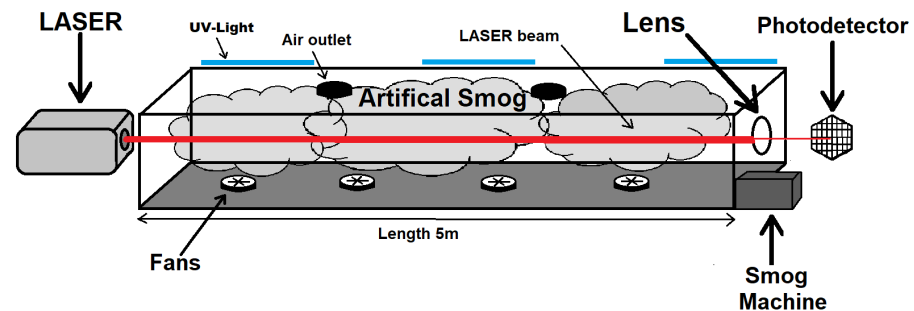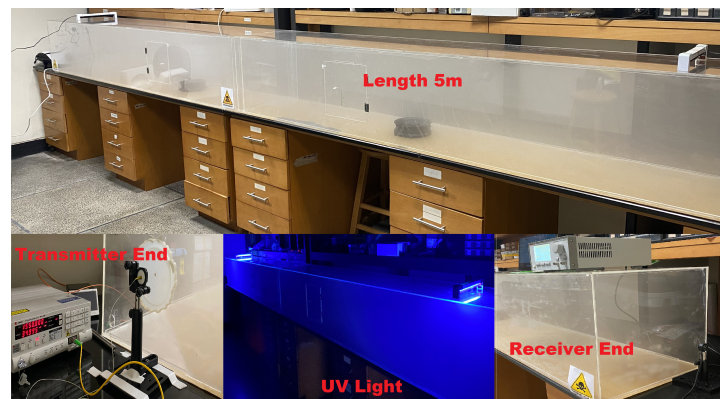

Figure 1. Block diagram.

Figure 2. Experimental setup for measuring smog attenuation.

Before conducting the experiments, the optical components are carefully calibrated to ensure accurate and reliable measurements. This includes aligning the laser beam path and optimizing the receiver sensitivity. Calibration procedures are performed iteratively to account for any drift or variations in the system parameters. The data collection involves systematically varying the density of the artificial smog within the chamber and recording the corresponding optical signal power levels at the receiver. The visibility increases with time as the smog in the chamber settles. The visibility inside the chamber can be measured using any of the two methods discussed in [24]. We use a broad-spectrum halogen light to measure the transmittance over the length of the chamber and then calculate the visibility index using $V = -10\log_{10}(T_{th})/\gamma_\lambda$. Standard visibility levels for different weather conditions can be found in [25]. Measurements are taken at regular intervals (after every 0.1 s) to ensure a comprehensive dataset. Additionally, control experiments are conducted without the presence of smog to establish a baseline reference. The experiment is repeated three times with the same controlled atmospheric conditions, and then the average of the datasets is used to analyze the system. Figure 3 shows the chamber with and without smog. The data points are categorized based on the smog density levels for the subsequent analysis. Table 1 shows the considered characteristics of the FSO system.

Figure 3. The 5 m chamber with and without smog.

Table 1. Properties of FSO.

Parameters	Laser 1	Laser 2
Wavelength	780 nm	1550 nm
Transmitted power	−3 dBm	10 dBm
Transmitter peak voltage	50 mV	30 mV
Power stability	±0.2 dB (typ.)	±0.01 dB (typ.)
Photodetector's spectral range	400–640 nm	800–1700 nm
Operating temperature	0–40 °C	15–35 °C
Photodetector's diameter	9.7 mm	9.7 mm
Response time	<1 µs	<1 µs

4. Result and Discussions

Figure 4 shows the measured smog attenuation (dB) against the observation time (approx. 50 min) for 780 nm and 1550 nm. Comparing the settling time of the smog with fog, it is observed that smog particles take more time to settle as compared to the fog [26,27]. This is because smog contains high concentrations of $PM_{2.5}$ particles, which are lighter as compared to water droplets in fog. The measured attenuation is higher at 780 nm than at 1550 nm for the given period. The result demonstrates a clear correlation between the wavelength and the extent of the signal degradation. We can also quantitatively describe the relationship between the smog density and optical signal attenuation. As the smog density decreases with time, a proportional decrease in the signal attenuation can be observed. There is an attenuation difference of 12 dB, 8 dB, and 3 dB for the two lasers at dense, moderate, and light smog, respectively, inside the chamber of a length of 6 m.
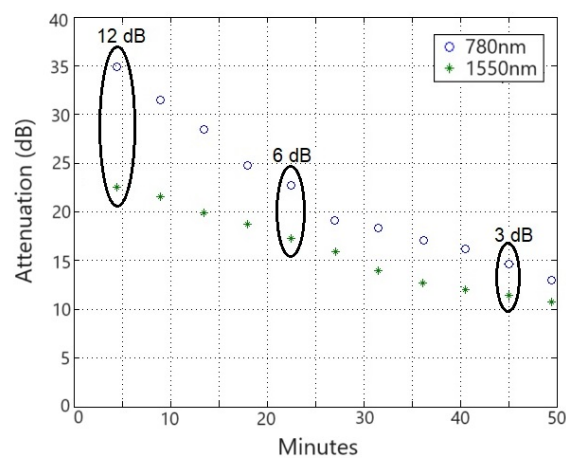

Figure 4. Attenuation (dB) versus observation time (minutes) for 780 nm and 1550 nm inside 6 m chamber.

Figure 5 shows the change in the specific attenuation for both wavelengths. It can be observed that the 1550 nm channel is more stable as compared to the 780 nm channel and has low magnitudes of a specific change in attenuation. There can be two reasons behind this behavior. (i) The 780 nm laser used has low power stability as compared to the 1550 nm laser as shown in Table 1. These fluctuations in the transmitted power can induce a profound effect on attenuation. (ii) The wavelength 780 nm is more vulnerable to smog channels and establishes an unstable optical link as compared to 1550 nm.
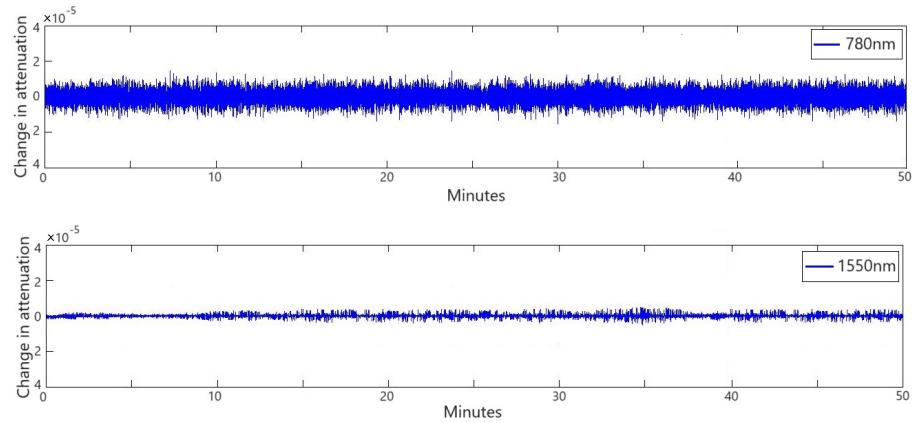

Figure 5. Change in attenuation over observation time (minutes).

The attenuation of an optical signal due to absorption and scattering is very much dependent on the size of the particulate matter (PM), recalling Equations (1) and (2). However, the modified Kim model has defined the value of q for fog and smoke in Equation (6), which shows the wavelength dependency of attenuation. Figure 6 shows that empirical exponential curve fitting is in good correlation with the measured received power. The goodness of fitting, quantified through metrics like the root mean square error (RMSE), serves as a crucial measure of how well any model aligns with the observed data. In our context, the close adherence of the data to the exponential law signifies the robustness of our analysis and implies that the signal attenuation follows an expected decay pattern. This adherence enhances the predictive capabilities, allowing for an accurate estimation of the received power. The slope of the 780 nm curve is smaller initially and then increases slightly with an increase in visibility. However, for 1550 nm, the slope of the curve is initially greater and reduces with time as the visibility increases.
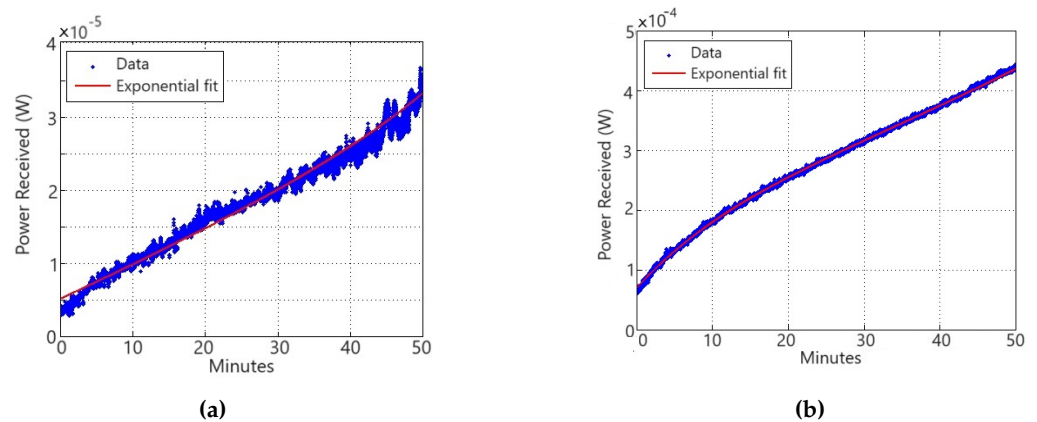

(a)　　　　　　　　　　　　　　　　　　　　　　　　**(b)**

Figure 6. Power received and its co-relation with exponential curve fitting for (**a**) 780 nm and (**b**) 1550 nm.

Figures 7 and 8 show a log–log plot for the smog attenuation against the visibility for the 780 nm and 1550 nm wavelengths. The log–log plot of the attenuation curve obtained

from the measured dataset shows good coherence with the proposed modified model defined by Equation (6). This indicates the wavelength dependency of smog attenuation as predicted by the modified Kim model. The plot also shows that the smog attenuation for the 780 nm wavelength is almost 125 dB/km, 105 dB/km, and 45 dB/km for dense, moderate, and light smog, respectively. The smog attenuation for the 1550 nm wavelength is almost 112 dB/km, 70 dB/km, and 35 dB/km for dense, moderate, and light smog, respectively. These measurements were carefully taken under artificial smog conditions wherein the visibility decreases linearly with time and is quite homogeneous in nature. Whereas, for outdoor measurements, the attenuation values can reach up to 120 dB/km for continental fog and up to 480 dB/km for maritime fog [28]. This is because of the fact that naturally occurring fog is not homogeneous and has different particle density patches throughout the length. The temperature, humidity, and wind vary randomly in outdoor environments and can cause significant attenuation.
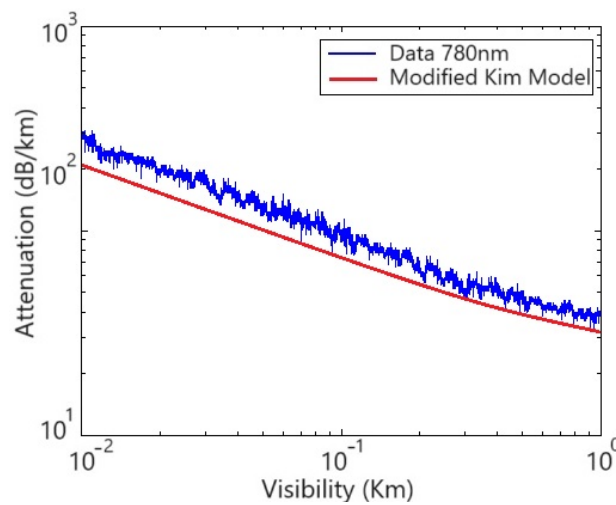

Figure 7. Measured smog attenuation versus the visibility for 780 nm.
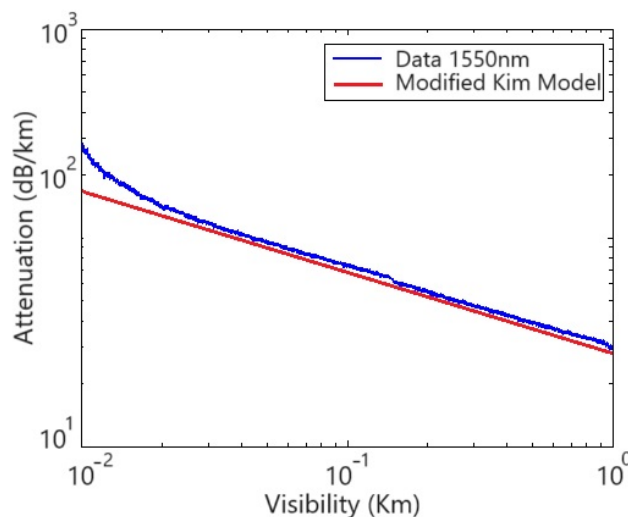

Figure 8. Measured smog attenuation versus the visibility for 1550 nm.

Comparing these results for smog attenuation with smoke and fog yields a better understanding of the FSO system in different environments. Table 2 shows a very interesting comparison between smog, smoke, and fog attenuation. For the 780 nm laser, the measured attenuation at V = 0.185 km for smog, smoke, and fog is 74 dB, 88 dB, and 102 dB, respectively. The attenuation decreases as the selected wavelength increases from 780

nm to 1550 nm. This is because a shorter wavelength scatters more in the atmosphere as compared to longer wavelengths. In all cases, the signal attenuates the most in fog as compared to smoke or smog. If the particle size is very small as compared to the wavelength, then the scattering of light is called Rayleigh scattering, whereas light scattered by larger particles undergoes Mie scattering [29]. Fog particles range from a few micrometers to tens of micrometers. In comparison with the operating lasers (0.78 and 1.55 micrometers), the size of the fog particles is generally larger than the wavelength and hence experiences Mie scattering.

Table 2. Comparison between smog, smoke, and fog. Data drawn for smoke and fog from [30,31], respectively.

Wavelength (nm)	Visibility (km)	Attenuation (dB/km)		
		Smog	**Smoke**	**Fog**
780	0.185	80	88	68
	0.245	65	69	40
1550	0.185	58	48	30
	0.245	48	39	23

Another interesting observation is that for 780 nm, the optical signal attenuates more in smoke as compared to smog, whereas, for 1550 nm, the smog attenuation is greater than the smoke attenuation. This is because of the difference in the composition and particle sizes of smoke and smog compared to the operating wavelength. Smoke particles are solid or liquid particles produced via the incomplete combustion of materials. The size of smoke particles can vary widely, from very small particles (nanoscale) to larger particles (microns) [32]. So, a lesser number of smoke particles experience Rayleigh scattering, and more particles experience Mie scattering for 780 nm, whereas for 1550 nm more particles follow Rayleigh scattering and lesser particles follow Mie scattering. However, smog particles vary widely in size, ranging from a few nanometers to several micrometers. Ultrafine particles, which are smaller than 0.1 micrometers, and fine particles (PM 2.5) with a diameter of 2.5 micrometers or smaller are both common in smog. So, a lesser number of smog particles experience Mie scattering and more particles experience Rayleigh scattering for 780 nm, whereas for 1550 nm almost all the particles follow Rayleigh scattering. Therefore, before selecting any wavelength for a particular environment, the composition and particle size distribution of air needs to be studied thoroughly to understand the behavior and strength of the scattering.

5. Conclusions

This paper demonstrates the impact of smog on FSO channels operating at 780 nm and 1550 nm. The wavelength-dependent model is tested for smog and optical attenuation and is compared with smoke and fog for the same laboratory-controlled conditions. The details to design an indoor chamber and methods to mimic a real outdoor environment as closely as possible are discussed. The experimental results of smog attenuation show that for 780 nm, the optical signal degradation is approximately 122 dB/km to 45 dB/km, and for 1550 nm, it ranges from 118 dB/km to 35 dB/km as the visibility increases. Comparing the measurements for three different environmental conditions, it is evident that smog experiences more attenuation as compared to smoke and fog. The result shows close validation with the modified Kim model, but a more accurate smog model can be derived using a real outdoor campaign.

Although FSO has been researched for decades now, still it faces challenges for its large-scale deployment around the globe. These challenges include designing compact-size FSO devices that can be integrated with all currently available IoT devices, the realization of a communication network, maximizing the energy efficiency while ensuring high performance, and developing suitable attenuation models for all atmospheric effects.

Abbreviations

The following abbreviations are used in this manuscript:

FSO	Free-Space Optics
LOS	Line Of Sight
PM	Particulate Matter
OWC	Optical Wireless Communication
EMI	Electromagnetic Interference
ITU	International Telecommunication Union
SNR	Signal-to-Noise Ratio
BER	Bit Error Rate
RF	Radio Frequency
VOC	Volatile Organic Compound
RH	Relative Humidity
UV	Ultraviolet
RMSE	Root Mean Square Error

References

1. Singhal, P.; Gupta, P.; Rana, P. Basic concept of free space optics communication (FSO): An overview. In Proceedings of the 2015 International Conference on Communications and Signal Processing (ICCSP), Melmaruvathur, India, 2–4 April 2015; pp. 0439–0442. https://doi.org/10.1109/ICCSP.2015.7322926.
2. Celik, A.; Romdhane, I.; Kaddoum, G.; Eltawil, A.M. A Top-Down Survey on Optical Wireless Communications for the Internet of Things. *IEEE Commun. Surv. Tutor.* **2023**, *25*, 1–45. https://doi.org/10.1109/COMST.2022.3220504.
3. Arya, S.; Chung, Y.H. A Comprehensive Survey on Optical Scattering Communications: Current Research, New Trends, and Future Vision. *IEEE Commun. Surv. Tutor.* **2023**, 1. https://doi.org/10.1109/COMST.2023.3339371.
4. Khalighi, M.A.; Uysal, M. Survey on Free Space Optical Communication: A Communication Theory Perspective. *IEEE Commun. Surv. Tutor.* **2014**, *16*, 2231–2258. https://doi.org/10.1109/COMST.2014.2329501.
5. Wei, B.; Shen, S.; Wang, G.; Zhang, H.; Tang, X.; Zhao, L. Applications of Free Space Optics in Terrestrial Backhaul. In Proceedings of the 2023 Asia Communications and Photonics Conference/2023 International Photonics and Optoelectronics Meetings (ACP/POEM), Wuhan, China, 4–7 November 2023; pp. 01–04. https://doi.org/10.1109/ACP/POEM59049.2023.10369134.
6. El-Mottaleb, S.A.A.; Mohamed, A.G.; Ahmed, H.Y.; Zeghid, M. Performance Enhancement of FSO communication system Under Rainy Weather Environment using a novel encryption technique. *IEEE Access* **2024**, *12*, 13729–13746. https://doi.org/10.1109/ACCESS.2024.3357396.
7. Khallaf, H.S.; Hashima, S.; Rihan, M.; Mohamed, E.M.; Kasem, H.M. Quantifying Impact of Pointing Errors on Secrecy Performance of UAV-Based Relay-Assisted FSO Links. *IEEE Internet Things J.* **2024**, *11*, 2979–2989. https://doi.org/10.1109/JIOT.2023.3297857.
8. Ciaramella, E.; Arimoto, Y.; Contestabile, G.; Presi, M.; D'Errico, A.; Guarino, V.; Matsumoto, M. 1.28 terabit/s (32 × 40 Gbit/s) wdm transmission system for free space optical communications. *IEEE J. Sel. Areas Commun.* **2009**, *27*, 1639–1645. https://doi.org/10.1109/JSAC.2009.091213.

9.   Colvero, C.P.; Cordeiro, M.C.R.; von der Weid, J.P. FSO systems: Rain, drizzle, fog and haze attenuation at different optical windows propagation. In Proceedings of the 2007 SBMO/IEEE MTT-S International Microwave and Optoelectronics Conference, Salvador, Brazil, 29 October–1 November 2007; pp. 563–568. https://doi.org/10.1109/IMOC.2007.4404328.

10.   Hu, S.; Liu, H.; Zhao, L.; Bian, X. The Link Attenuation Model Based on Monte Carlo Simulation for Laser Transmission in Fog Channel. *IEEE Photonics J.* **2020**, *12*, 1–10. https://doi.org/10.1109/JPHOT.2020.3006853.

11.   El-Nayal, M.K.; Aly, M.M.; Fayed, H.A.; AbdelRassoul, R.A. Adaptive free space optic system based on visibility detector to overcome atmospheric attenuation. *Results Phys.* **2019**, *14*, 102392. https://doi.org/https://doi.org/10.1016/j.rinp.2019.102392.

12.   Aborisade, O.; Ojo, J.; Owolawi, P.; Adedayo, K. Prediction of Attenuation using Visibility variations and other Meteorological Parameters in George, Western Cape, South Africa. *IOP Conf. Ser. Earth Environ. Sci.* **2021**, *665*, 012053. https://doi.org/10.1088/1755-1315/665/1/012053.

13.   Verdugo, E.; Da Silva Mello, L.; Pereira Colvero, C.; Nebuloni, R. Estimation of Rain Attenuation in FSO Links based on Visibility Measurements. In Proceedings of the 2023 17th European Conference on Antennas and Propagation (EuCAP), Florence, Italy, 26–31 March 2023; pp. 1–5. https://doi.org/10.23919/EuCAP57121.2023.10133748.

14.   Djordjevic, I.B. Adaptive Modulation and Coding for Free-Space Optical Channels. *J. Opt. Commun. Netw.* **2010**, *2*, 221–229. https://doi.org/10.1364/JOCN.2.000221.

15.   Khalid, H.; Muhammad, S.S.; Nistazakis, H.E.; Tombras, G.S. Performance Analysis of Hard-Switching Based Hybrid FSO/RF System over Turbulence Channels. *Computation* **2019**, *7*, 28. https://doi.org/10.3390/computation7020028.

16.   Baiwa, R.; Verma, P. Performance Analysis of FSO System for Advanced Modulation Formats Under Different Weather Conditions. In Proceedings of the 2018 Second International Conference on Intelligent Computing and Control Systems (ICICCS), Madurai, India, 14–15 June 2018; pp. 1490–1495. https://doi.org/10.1109/ICCONS.2018.8663090.

17.   Bajwa, R.; Verma, P. Effect of Different Atmospheric Conditions on the Performance of the FSO System at 1550 nm. In Proceedings of the 2018 5th International Conference on Signal Processing and Integrated Networks (SPIN), Noida, India, 22–23 February 2018; pp. 390–395. https://doi.org/10.1109/SPIN.2018.8474154.

18.   Amarasinghe, Y.; Zhang, W.; Zhang, R.; Mittleman, D.M.; Ma, J. Attenuation of Terahertz Waves by Wet Sn Ow, Dry Snow and Rain. In Proceedings of the 2020 IEEE International Conference on Plasma Science (ICOPS), Singapore, 6–10 December 2020; pp. 216–216. https://doi.org/10.1109/ICOPS37625.2020.9717532.

19.   Whitten, G. The chemistry of smog formation: A review of current knowledge. *Environ. Int.* **1983**, *9*, 447–463. https://doi.org/https://doi.org/10.1016/0160-4120(83)90003-X.

20.   Raza, W.; Saeed, S.; Saulat, H.; Gul, H.; Sarfraz, M.; Sonne, C.; Sohn, Z.H.; Brown, R.J.; Kim, K.H. A review on the deteriorating situation of smog and its preventive measures in Pakistan. *J. Clean. Prod.* **2021**, *279*, 123676. https://doi.org/https://doi.org/10.1016/j.jclepro.2020.123676.

21.   McWhorter, T.M.; Shrestha, S. System for Monitoring Air Quality and Smog. In Proceedings of the 2018 IEEE International Conference on Electro/Information Technology (EIT), Rochester, MI, USA, 3–5 May 2018; pp. 0415–0419. https://doi.org/10.1109/EIT.2018.8500287.

22.   Ijaz, M.; Ghassemlooy, Z.; Pesek, J.; Fiser, O.; Le Minh, H.; Bentley, E. Modeling of Fog and Smoke Attenuation in Free Space Optical Communications Link Under Controlled Laboratory Conditions. *J. Light. Technol.* **2013**, *31*, 1720–1726. https://doi.org/10.1109/JLT.2013.2257683.

23.   Liu, A.; Wang, H.; Cui, Y.; Shen, L.; Yin, Y.; Wu, Z.; Guo, S.; Shi, S.; Chen, K.; Zhu, B.; et al. Characteristics of Aerosol during a Severe Haze-Fog Episode in the Yangtze River Delta: Particle Size Distribution, Chemical Composition, and Optical Properties. *Atmosphere* **2020**, *11*, 56.

24.   Ijaz, M.; Ghassemlooy, Z.; Perez, J.; Brazda, V.; Fiser, O. Enhancing the Atmospheric Visibility and Fog Attenuation Using a Controlled FSO Channel. *IEEE Photonics Technol. Lett.* **2013**, *25*, 1262–1265. https://doi.org/10.1109/LPT.2013.2264046.

25.   Ojo, J.; Olaitan, J.; Ojo, O. Characterization of fog-induced attenuation for optimizing optical propagation links in Nigeria. *Results Opt.* **2022**, *9*, 100279. https://doi.org/https://doi.org/10.1016/j.rio.2022.100279.

26.   Khadapkar, K.P. A study of a smog-fog-smog cycle and the processing of PAH and oxy-PAH by a fog cloud. Master's Thesis, Louisiana State University, Baton Rouge, LA, USA, 2011.

27.   Ijaz, M.; Ghassemlooy, Z.; Rajbhandari, S.; Le Minh, H.; Perez, J.; Gholami, A. Comparison of 830 nm and 1550 nm based free space optical communications link under controlled fog conditions. In Proceedings of the 2012 8th International Symposium on Communication Systems, Networks & Digital Signal Processing (CSNDSP), Poznan, Poland, 18–20 July 2012; pp. 1–5. https://doi.org/10.1109/CSNDSP.2012.6292739.

28.   Muhammad, S.S.; Flecker, B.; Leitgeb, E.; Gebhart, M. Characterization of fog attenuation in terrestrial free space optical links. *Opt. Eng.* **2007**, *46*, 066001. https://doi.org/10.1117/1.2749502.

29.   Mao, T.P.; Zhou, D.F.; Niu, Z.X. The calculation model of the attenuation due to clouds or fog and the analysis of its characteristic. In Proceedings of the 2004 Asia-Pacific Radio Science Conference, Qingdao, China, 24–27 August 2004; pp. 332–334. https://doi.org/10.1109/APRASC.2004.1422475.

30.   Ijaz, M.; Ghassemlooy, Z.; Gholami, A.; Tang, X. Smoke attenuation in free space optical communication under laboratory controlled conditions. In Proceedings of the 7'th International Symposium on Telecommunications (IST'2014), Tehran, Iran, 9–11 September 2014; pp. 758–762. https://doi.org/10.1109/ISTEL.2014.7000804.

31. Fatima, K.; Muhammad, S.S.; Leitgeb, E. Adaptive coded modulation for FSO links. In Proceedings of the 2012 8th International Symposium on Communication Systems, Networks & Digital Signal Processing (CSNDSP), Poznan, Poland, 18–20 July 2012; pp. 1–4. https://doi.org/10.1109/CSNDSP.2012.6292700.

32. Imran, H.; Maqsood, Z.; Ullah, A.; Butt, N.Z. Effective Prediction of Transmission of Solar Irradiance through Dusty Solar Panels using Atmospheric Aerosol Data for Lahore, Pakistan. In Proceedings of the 2019 IEEE 46th Photovoltaic Specialists Conference (PVSC), Chicago, IL, USA, 16–21 June 2019; pp. 2889–2893. https://doi.org/10.1109/PVSC40753.2019.8980728.